AGU PUBLICATIONS

Water Resources Research

RESEARCH ARTICLE
10.1002/2016WR019421

Experimental investigation of clogging dynamics in homogeneous porous medium

Jikang Shen[1] and Rui Ni[1]

[1]Department of Mechanical and Nuclear Engineering, Pennsylvania State University, University Park, Pennsylvania, USA

Key Points:
- We propose a novel experimental method to track particle dynamics in 3-D porous medium during clogging
- The method shows the time evolution and spatial distribution of clogged pores
- It provides statistics of particle velocity distribution and displacement over time

Supporting Information:
- Supporting Information S1
- Movie S1

Correspondence to:
R. Ni,
rxn5006@engr.psu.edu

Citation:
Shen, J., and R. Ni (2017), Experimental investigation of clogging dynamics in homogeneous porous medium, *Water Resour. Res.*, *53*, 1879–1890, doi:10.1002/2016WR019421.

Received 28 JUN 2016
Accepted 8 FEB 2017
Accepted article online 11 FEB 2017
Published online 3 MAR 2017

Abstract A 3-D refractive-index matching Lagrangian particle tracking (3D-RIM-LPT) system was developed to study the filtration and the clogging process inside a homogeneous porous medium. A small subset of particles flowing through the porous medium was dyed and tracked. As this subset was randomly chosen, its dynamics is representative of all the rest. The statistics of particle locations, number, and velocity were obtained as functions of different volumetric concentrations. It is found that in our system the clogging time decays with the particle concentration following a power law relationship. As the concentration increases, there is a transition from depth filtration to cake filtration. At high concentration, more clogged pores lead to frequent flow redirections and more transverse migrations of particles. In addition, the velocity distribution in the transverse direction is symmetrical around zero, and it is slightly more intermittent than the random Gaussian curve due to particle-particle and particle-grain interactions. In contrast, as clogging develops, the longitudinal velocity of particles along the mean flow direction peaks near zero because of many trapped particles. But at the same time, the remaining open pores will experience larger pressure and, as a result, particles through those pores tend to have larger longitudinal velocities.

1. Introduction

In nature, underground water and oil often contain solid contents, such as small colloid-size particulates [*Chen et al.*, 2010], microorganisms [*Drummond et al.*, 2015], or larger sand particles. The transport dynamics of these particle-laden flow in porous medium significantly differ from that of pure liquid. One of the resulting issues is the clogged porous medium induced by particle deposition and accumulation. In petroleum engineering, observations show that particle plugging near wellbores can reduce permeability and well productivity [*Porter et al.*, 1989]. In wastewater treatment, the early surface clogging of filters sharply decreases the filtration efficiency and increases energy consumption [*Song et al.*, 2006; *Rodgers et al.*, 2004]. A fundamental understanding of the clogging dynamics is essential in predicting and avoiding unwanted clogging occurrences.

The study of clogging phenomena is commonly addressed with filtration process. This process is known to be very sensitive to the size ratio d_g/d_p between the grains d_g that constitute the porous medium and fine particles (d_p) in the liquid. Based on this ratio, there are many filtration mechanisms that have been identified, including surface cake, straining, and physicochemical filtration [*McDowell-Boyer et al.*, 1986]. Large particles ($d_g/d_p < 1$) cannot enter the porous medium, so they will accumulate on the surface instead and form a filter cake. A filter cake has a very low permeability and causes large pressure drop [*Willis and Tosun*, 1980]. In contrast, small particles will penetrate deep into the porous medium through many pores, but they can still be filtered out for many reasons, one of which is straining [*Corapcioglu and Haridas*, 1984; *McDowell-Boyer et al.*, 1986; *Ginn et al.*, 2002]. Straining occurs when fine particles are trapped in pore throats. Once it starts, straining triggers a chain reaction: the trapped particles will serve as additional collectors to capture more particles, and so forth until the pore gets completely clogged [*O'Melia and Ali*, 1978; *Bradford et al.*, 2002]. *Sakthivadivel and Einstein* [1970] found that the straining is most likely to occur in the range of $10 < d_g/d_p < 20$. The permeability reduction caused by straining is not as severe as that in filter cake because transport can still occur in larger pores [*Bradford et al.*, 2002]. However, straining near the surface of porous medium is very likely to lead to the formation of cake [*McDowell-Boyer et al.*, 1986]. Physicochemical filtration plays a significant role when fine particles are very small in both their absolute sizes and relative sizes, comparing with grains [*McDowell-Boyer et al.*, 1986; *Ives*, 1970; *Bradford et al.*, 2002]. At this

small physical scale, multiple transport and attachment mechanisms play more important roles than straining [*Yao et al*., 1971; *McDowell-Boyer et al*., 1986].

Theoretical study has been developed to gain insights into the physical process of particle captured in porous media [*Molnar et al*., 2015]. *Rajagopalan and Tien* [1976] calculated the particle trajectories by using streamline functions and force balance to predict the initial filtration efficiency and pressure drop across the filter. There are many experimental works as well in order to study the dynamics of particle capture. Due to the opacity of porous media, majority of experiments investigated clogging based on quantities such as head loss and effluent particle concentration through the porous media. Factors such as flow rate, grain size [*Kau and Lawler*, 1995; *Hunt et al*., 1993], influent particle size distribution [*Mackie and Bai*, 1992], and particle chemical properties [*Hajra et al*., 2002] were also studied to obtain an overall understanding of the clogging behavior. On the other hand, a few noninvasive experimental techniques have been developed to visualize the porous media. Some are in quasi-2-D micromodels [*Auset and Keller*, 2006]. X-ray tomography has been proven to be efficient to reconstruct the 3-D internal structure of granular beds with high spatial resolution [*Seidler et al*., 2000]. However, the attenuation of radiation through the porous medium can cause large errors especially when the sample is large [*Wildenschild et al*., 2002]. Nuclear magnetic resonance (NMR) imaging techniques have also been used to obtain velocity fields [*Kutsovsky et al*., 1996], but their spatial and temporal resolutions may not be high enough in complicated suspensions with time-dependent response [*Fukushima*, 1999]. Above all, most of these experiments cannot track individual particle to understand the clogging dynamics.

A visualization technique that can overcome this opaque material problem is the refractive index matching (RIM). Over decades, protocols of achieving RIM and a list of RIM materials and their properties have been proposed by researchers and summarized by *Wiederseiner et al*. [2011] and *Dijksman et al*. [2012]. This method has been successfully implemented in the water resources community. Examples include microbial biofilm transport [*Leis et al*., 2005] and velocity field measurement [*Datta et al*., 2013].

In an optical-accessible RIM, classic techniques such as particle image velocimetry (PIV) and Laser Doppler velocimetry (LDV) can be applied. PIV system has been used mostly in 2-D micromodels [*Kazemifar et al*., 2015a; *Auset and Keller*, 2006] and it can only provide velocity measurements at the fixed locations. To study particle dynamics in the Lagrangian framework, Lagrangian particle tracking (LPT) system was successfully implemented in RIM before to provide 3-D tracer trajectories in a unclogged medium [*Moroni and Cushman*, 2001; *Huang et al*., 2008; *Lachhab et al*., 2008] and most efforts were devoted to quantifying the flow pattern and velocity distributions.

The clogging dynamics is a time-varying process by nature. The clogged pores induced by fine particles will redirect the flow and, in turn, affect the fine particles motion. This complex process poses significant challenges to the experimental method. This explains why most previous experiments rely on pressure and flow rate measurement without attempting any statistics that relate to the local and instantaneous dynamics inside the porous medium. Yet these statistics are crucial to validate models and pinpoint the key mechanisms of clogging. In this paper, we build an inexpensive 3-D-RIM-LPT system to provide statistics on motions of fine particles during clogging. These statistics could potentially shed new lights on problems for water resources and petroleum and help to avoid unwanted early clogging.

2. Experimental Methods

2.1. Refractive Index Match

The internal view of the porous medium is provided by matching the refractive indices of liquid, porous medium, and fine particles in the flow. Several standard refractive-index-matching liquids and solids have been summarized by *Dijksman et al*. [2012]. From that list, water and hydrogels made from Polyacrylamide are chosen for this experiment.

Figure 1a shows many hydrogels covering the bottom of a beaker with a grid underneath. The grid spacing is 10 mm and the width of the grid line is 1 mm. These two numbers are chosen to compare with the size of two typical hydrogels shown in the figure: eight large beads (10–30 mm, purchased from Educational Innovations) and several layers of small particles ($\sim$1 mm, purchased from JRM Chemical). Large beads are used to construct the porous medium and fine particles are utilized to clog the porous medium. Note that it

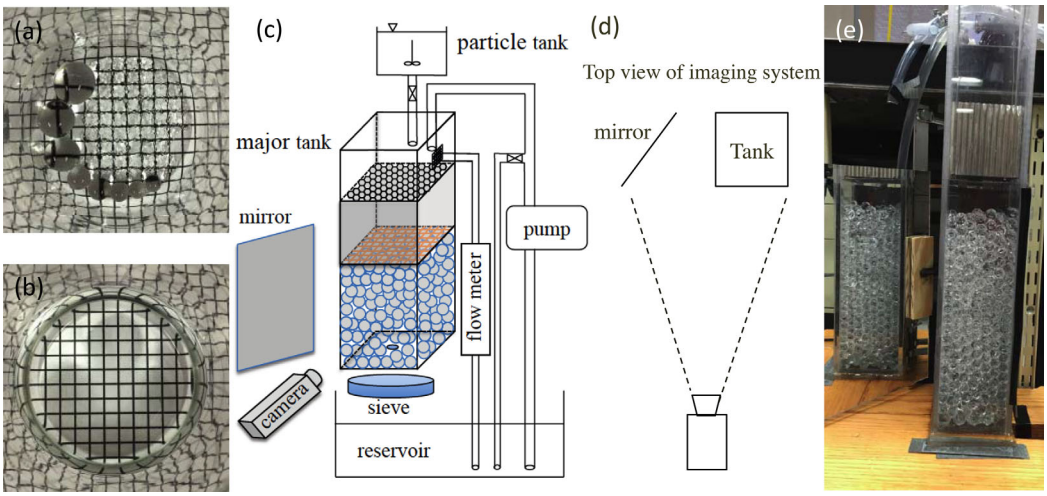

Figure 1. (a, b) Index matching hydrogel beads with water. Figure 1a shows a beaker containing several large hydrogel beads and a few layers of small particles. In Figure 1b, we have added just enough water to cover the beads. The hydrogel-water mixture is optically transparent. (c) Schematic of the experimental setup and (d) top view of the imaging system to show how mirror provides a second view of the tank. (e) A picture of the tank and the mirror captured by the front camera.

is difficult to see individual small particle. But they manifest their presences from the distorted view of the grid due to the mismatch of the refractive indices between fine particles and air. In this experiment, many large beads with a diameter of 12.24 ± 0.55 mm are chosen to create the homogeneous porous medium. The flow through this porous medium is seeded with a high concentration of 1.07 ± 0.41 mm fine particles. A good refractive index matching is confirmed with the disappearance of both large beads and small particles after immersion in water in Figure 1b. Note that the particle size is much larger than the colloid limit, so in this work we do not consider Brownian motion or surface attachment due to electrostatic forces.

When everything is optically transparent, we will need to mark a subset of fine particles to track. Polyacrylamide hydrogels are prepared by soaking them with large amount of distilled water. When water dyed with fluorescein sodium salt (F6377 from Sigma–Aldrich), hydrogel will absorb fluorescein as well, providing a way to make themselves visible again. The concentration of fluorescent particles must be low enough that no two particles overlap with each other, but high enough that they can explore many clogged pore throats, thereby allowing us to collect sufficient statistics about the number of clogs. In our experiment, 0.05% volumetric concentration is chosen to meet these two criteria.

2.2. Experimental Setup

A schematic of the experimental setup is provided in Figures 1c and 1d. The entire setup consists of two major parts: the fluid flow system and the imaging system.

2.2.1. Fluid Flow System

The column is made of acrylic sheets and has inner dimensions of 8 cm $\times$ 8.6 cm $\times$ 61.0 cm. Type II deionized water with conductivity around 1.0 μS cm^{-1} is driven by a constant hydrostatic pressure head through the permeable bed. A recirculation diaphragm pump (model No. SHURflo 2088-594-154) provides a constant flow rate to the column; as soon as permeability reduces, extra water that cannot flow through the main column was directed to a bypass hole located near the top of the column in order to maintain a constant hydrostatic pressure head. The variation of the pressure is due to the finite size of the bypass hole, which is about 1.1 cm diameter. Comparing with the total hydrostatic head 52.6 cm, it creates a head fluctuation around 2.1%. Since this variation is small, we consider this is a constant-head measurement. The flow rate through the bypass hole increases over time as flow rate decreases in the main column as a result of reduced permeability. The flow rate through this bypass hole is measured by a flowmeter (model: FTB602B, Omega Engineering, Inc.). The flow rate over the entire column is about $Q = 106.0$ mL/s, and it decreases to about $<11\%$ of the original Q by the end of the experiment. The hydraulic conductivity is defined as $K = QL/Ah$, where Q, L, A, and h represent volumetric flow rate, length and cross-sectional area of porous bed, and the pressure head, respectively. For our system at a constant pressure head ($\pm 2\%$), the decrease in flow rate will be translated to the decrease in the hydraulic conductivity, from 1.2 cm/s (3.78×10^5 m/yr)

to 0.13 cm/s (4.16 $\times 10^4$ m/yr). This hydraulic conductivity is comparable to the one of gravel at $10^4 \sim 10^7$ (m/yr). From the flow rate, the Reynolds number based on the superficial velocity v can be determined $Re = \rho D_p v/\mu \approx 184.8$ in a clean porous medium, but it will decrease to $Re \approx 20.3$ when it is clogged. Comparing with the critical Reynolds number around 40–80 [*Chilton and Colburn*, 1931], the non-Darcy effect in our experiment is not negligible in the very beginning but becomes a relatively small effect near the end. However, the focus of the study is about the straining-induced clogging that relies mostly on the size ratio between grain and small particles rather than their own physical sizes, so the Reynolds number effect might not be that important. But this hypothesis needs to be tested in future in order to be more conclusive.

The particles are injected into the column through a particle tank, which is stirred mechanically to achieve a uniform particle concentration. The particle tank is driven by its own pressure, so the particle feeding rate is always maintained constant even the overall flow rate is decreasing due to clogging. The experiments have been repeated in seven different particle concentrations ϕ. The particle concentration is an average number calculated using the total volume of particles divided by the total volume of water flowed through the column over the entire experiment. The concentrations are $\phi = 1.40$, 2.02, 2.65, 3.18, 3.87, 4.39, and 4.91%.

To distribute particles and flow uniformly across the entire cross-sectional area, the water flow and particle flow will impact on a perforated plate that has a dimension of 7 cm $\times$ 6.5 cm $\times$ 0.6 cm with 20 circular holes of 5.6 mm diameter each. After the perforated plate, the flow will go through a honeycomb layer to straighten the flow and minimize the secondary flow. The honeycomb has a unit cell size of 6.2 mm with length 76.4 mm and aspect ratio 12.32. The lower part of the tank is the test section packed with hydrogel beads. To fix the porous medium during experiment, the packed beads are confined by a mesh, with 7 mm $\times$ 7 mm square holes separated by 1 mm width wires. The mesh has only 2% solidity, which should not affect the clogging dynamics, yet it is sufficient to maintain the 12.24 mm large grain in place. The volume **V** of the entire porous medium is 8.6 cm $\times$ 8.0 cm $\times$ 29.5 cm. The porosity is estimated to be 0.36 by dividing the volume of the interstitial water by **V**. This value falls in the range of random close packing of monodispersed beads calculated by *Berryman* [1983]. Figure 1e shows the column filled with packed beads but no water. Once immersed in water, the entire column will be transparent. There is a drainage hole of 6 mm diameter at the bottom. A layer of glass beads is paved on top of the hole to prevent accidental blockage by 12 mm hydrogel bead. Experimental observations show that clogging barely reaches all the way down to the glass bead layer. Thus, this layer is not a region of interest and is not likely to have much effect on the flow field above.

The water flowing through the porous medium is recirculated by a system, which mainly consists of a pump, a reservoir, and a sieve. The effluent out of the tank is filtered by a 125 μm sieve to make sure only pure water back to the recirculation, because any particles that go back to the pump will be crushed.

2.2.2. Imaging System

The key components of the imaging system are a Canon EOS 650D camera, a flat mirror, and two LED lamps. As shown in Figure 1d, the mirror serves as a virtual camera to provide a second view from side. Figure 1e shows one image captured by the front camera. The water column is in the middle of the image. The left column is just a reflection of the left side of the same column from the mirror. The image resolution is 1080 $\times$ 1920, which covers an area of 24.84 $\times$ 44.16 cm^2 with magnification about 0.23 mm/pixel. Similar methods have been proposed and successfully implemented in 3-D-PTV previously [*Putze*, 2005; *Willneff and Maas*, 2000]. There are three advantages of this design: (1) it is inexpensive comparing with methods utilizing multiple cameras; (2) one-camera design eliminates the needs for synchronization; and (3) imaging a high-aspect-ratio water column only utilizes very limited area of camera sensor. Including one more image from the mirror will solve this problem and save some storage space. Comparing with previous studies [*Putze*, 2005; *Willneff and Maas*, 2000], our imaging system provides only two views of the system instead of four views. As a result, the number of particles that can be tracked at each time using our system is limited to 10–20. Calibrating the positions of camera and mirror can be achieved with a similar method used before [*Ni et al*., 2012]. The difference is that the calibration target with many dots of known positions will be put in this packed hydrogel beads that are filled with water. Any distortions due to even the slightest refractive index mismatch will be included in this calibration process. It turns out that the error of particle position is around 0.3–0.5 mm in the transverse direction and 1.8 mm in the longitudinal direction along the flow. This type of error in the longitudinal direction is large because of the long distance in that direction. This long distance leads to a large angle of refraction at the surface of the tank, resulting in a systematical position

bias. The points near the top and bottom corners suffer more from this type of bias. However, this bias does not necessarily translate to velocity uncertainty, since it systematically affects the position measurements at all time steps. The uncertainty of velocity measurement is actually more sensitive to the random error, induced by the refractive index mismatch. It should be similar in all three directions as the system is isotropic. In our case, we can estimate this error using the calibration error along the transverse directions, i.e., 0.3–0.5 mm. At frame rate 30 fps, this will result in velocity uncertainty around $9-15$ mm/s, if we only take two consecutive positions to derive the velocity. Applying filter over nine frames to acquire the local velocity is a higher-order method [*Ni et al*., 2012], known to result in a much smaller velocity uncertainty <3 mm/s. As the errors are dominated by the small refractive-index mismatch, we choose to use only two views instead of four views [*Putze*, 2005; *Willneff and Maas*, 2000], as more views may not help to reduce this type of error by much.

More details of the particle tracking system and the algorithm can be found in *Ni et al*. [2012] and *Ouellette et al*. [2006, and references therein]. Here we briefly introduce the procedure of the data acquisition and analysis. Images captured by the camera will be separated into two parts, left part for mirror view and right part for the front view. The center position of fluorescent particles in both images can be fitted with a Gaussian profile or determined by averaging all pixel positions. The results from both methods are almost the same. After image processing, the triangulation step is achieved by projecting a line of sight from each particle center to the three-dimensional space based on the calibrated view parameters, and the intersection of two lines of sight from two different camera views determines the 3-D position of the particle. Once three-dimensional locations of many particles are acquired over time, the tracking is conducted by connecting those particles from one frame to another. Particles in the first few frames are linked by searching their nearest neighbors in the next frame. With three particles in one trajectory, the particle in the next frame will be added to the trajectory if adding this particle will not change the trajectory acceleration significantly (four frames method) [*Ouellette et al*., 2006]. This is based on the argument that the particle trajectory should be continuous with finite local jerk (rate of change of acceleration). Along each trajectory, random errors induced by the refractive-index mismatch will be significantly reduced by introducing a Gaussian filter. Finally, the smoothed trajectory will be differentiated over time to obtain the velocity of the particles [*Ni et al*., 2012]. Note that the errors in this experiment do not depend on the concentration of particles in the flow, since the number of dyed particles is kept the same throughout all the experiments, in spite of a much larger concentration of undyed fine particles.

Two LED lamps are placed above the column to provide uniform light on the entire test section. The blue LED lamps are designed by ourselves. Each lamp has an array of 4×7 blue LED bulbs, purchased from Sunshine Opto-electronics. Each bulb can provide 45 Lumen diffused light. The blue light in this experiment has a wavelength of 460–470 nm. Accordingly, the selected fluorescent dye has an excitation wavelength of 460 nm (blue light) and an emission wavelength of 515 nm (green light). The camera is adjusted and fixed till it captures the image of both the front of the tank and the side from mirror reflection. Video camera frame rate is fixed at 30 fps in all experiments, which is sufficient to capture the motion of even the fastest particles.

2.3. Experimental Procedures

Movie 1 in the auxiliary file shows the entire clogging process for concentration $\phi = 1.40$ and 4.91%. The experiment starts with a clean porous medium at time t_0 and, at that time, the water level just touches the bottom of the bypass hole. As more particles flowing through the porous medium, clogging starts to develop, permeability of the porous medium drops, and more flow is directed through the bypass hole. The pressure drop exerts more force on the porous medium due to pressure buildup resulted from the permeability reduction, and that is sufficient to compress the porous medium formed by hydrogels. The experiment ends at time t_1 when the bypass hole is fully immersed in water, indicating the permeability of the porous medium decreases from 1.6×10^3 d to 1.7×10^2 d. The high-concentration influent leads to a much fast clogging process (smaller t_1) comparing with the small-concentration case. After that, the pump stops and the water starts to drain from the bottom hole. The time of water level drop from the top of the entire column to the top of the test section is recorded as t_2, which is an indication of the permeability of the final state of the porous medium $\sim1.7\times10^2$ d. Once the two steps are finished, the honeycomb and mesh are removed and the porous medium is carefully flushed with water jet for multiple times. The jet causes some vertical motions of the grains, during which the pores are unclogged and the fine particles are flushed out.

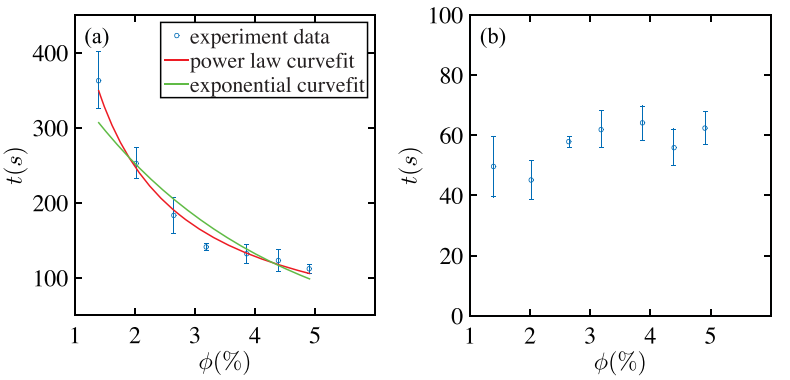

Figure 2. (a) Clogging time t_1 and (b) drainage time t_2 at different particle concentrations ϕ. In Figure 2a, open circles indicate the experimental data and red and green curves show the power law and exponential fit to the data.

The effluent is filtered with the same sieve. The collected particles were dried and their total volume is measured. The ratio between this volume to the interstitial volume in the porous medium is the specific deposit, which is used to quantify the permeability change during clogging. In our experiment, this ratio changes from 27.3 to 47.9%. However, from what we observed, the extra 20% increase may not entirely come from more deposited particles deep in the porous medium. Instead, they accumulated on the top surface as a result of cake filter development.

As more pores are clogged, the number of trapped particles becomes larger and larger. This will affect the particle tracking system as the system can only track limit amount of particles. To solve this problem, the images of trapped particles are removed by subtracting the background images averaged from last 50 frames. If the particle is not moving in last 50 frames, we consider it to be trapped and it does not need to be tracked anymore unless it starts to move again later.

3. Results and Discussion

The ratio of grain size to particle size in this experiment is $12.24/1.07=11.4$, which falls in the straining dominated regime reported by *Sakthivadivel and Einstein* [1970]. On the other hand, *Ives* [1970] reported that for dilute suspensions (less than 500 mg/L) of particle sizes ranging from 0.1 to 50 μm, physicochemical processes dominate the filtration process, while larger particles rely on straining. Since the particle size in this experiment is in millimeter scale, we believe that the dominating clogging mechanism is straining and mechanical clogging. Besides, *Ives* [1970] also addressed that cake filtration is more likely to happen at higher particle concentrations and *McDowell-Boyer et al*. [1986] mentioned that straining near the surface of porous media tends to lead to the formation of filter cakes. Thus, cake filtration is believed to be another clogging mechanism in this experiment.

Both grain size and particle size in our experiments are significantly larger than those in many environmental flow applications with nano or micron-sized colloids clogging the permeable beds with similar pore size [*Molnar et al*., 2015]. Our experiments will not be able to test all mechanisms for colloid particle clogging. But we believe that the insights gained from our experiments might be useful to understand straining of colloid particle in porous medium, as straining depends primarily on size ratio between grain and fine particle rather than their own physical sizes.

The clogging time t_1 and drainage time t_2 are shown as functions of concentration in Figure 2. In Figure 2a, each error bar indicates the uncertainty estimated from the standard error of at least five independent experiments. Since the dominant clogging mechanism in this experiment is straining, pores are more likely to be clogged when exposed to more particles. As expected, the clogging time decreases as particle concentrations increases due to less time for the ripening process [*O'Melia and Ali*, 1978]. The trend has been fitted with exponential curve (green) and power law (red). One may see that the experimental data fits much better with a power law relationship.

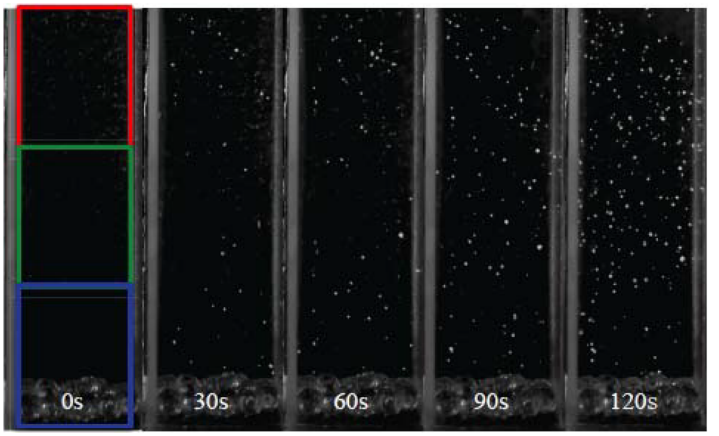

Figure 3. The time sequences of the development of clogging illustrated with many dyed particles at concentration ϕ=4.91%. At t = 0 s, three boxes with different colors showing three different subvolumes to use later in Figure 4.

The drainage time t_2 is shown in Figure 2b. Within the experimental uncertainty, the trend is almost flat with a weak transition from short to long drainage time at $\phi \approx 2.65\%$. From the experimental observations, one possible explanation of this transition is the difference in clogging patterns. At low particle concentrations, the depth filtration with most clogged sites located deep in the porous medium dominates. In this regime, the permeability decrease is mainly due to pure straining [*Bradford et al.*, 2002]. At high particle concentrations, similar straining process will happen, but only in a shallower region. These clogging sites near the top surface of the porous medium can lead to the formation of a filter cake with a lower permeability [*McDowell-Boyer et al.*, 1986]. In addition, even the experiment stops, there are some particles already suspending in the water column. The sediment of these particles thickens the cake and further slows down the drainage process. This clogging pattern is also confirmed by the experimental observations at high concentrations.

Figure 3 shows the development of clogging at concentration ϕ=4.91%. At t = 0 s, there is no particle in the porous medium. The tank is equally divided into three regions shown by three colors to facilitate later discussion. At later time, the bright dots show the positions of the dyed particles trapped in the porous medium. Since the volume ratio of dyed particles is only 0.05%, each dyed particle represents over a thousand invisible RIM particles. At t = 30 s, it seems that many clogged particles tend to form clusters, which suggests new clogged pores are more likely to be around existing ones. Those clusters will redistribute the flow pattern and that will lead to clogging in different places. We also observed some temporary unclogging and reclogging due to local pressure buildup and flow redirection. At t = 120 s, the system is fully clogged with more particles being trapped in the upper half region due to more incoming particles from the top.

The transition of clogging patterns can also be demonstrated in Figure 4. It shows the time evolution of number of dyed particles *N*. The column is divided into three regions as shown in Figure 3 at t = 0. The same colors for different subareas are used here for different curves. In all three Figures 4a–4c, the gradual increase of N with time indicates the development of clogged pores in the porous medium. Figure 4a refers to the particle concentration at ϕ=2.02%. In the first 50 s, the amount of particles trapped in the top part is larger than the other two. This is because the top part is always exposed to high-concentration incoming influent, so the clogging is more likely to develop there first. Sometimes clogged pores may be unclogged due to the pressure buildup, which is indicated by the fluctuations of the curve. Although three curves overlap for the first 100 s, after 125 s, more particles are trapped in the middle and lower region of the tank, suggesting that more clogged pores are located in deep bed. This agrees with the experimental observations and our discussions about Figure 2b.

Figure 4b refers to the particle concentration at ϕ=2.65%. Although the increasing trend remains the same, the red curve tends to stay above the other two curves, implying that more particles are trapped near the top before they can reach deep. After 100 s, the gap between the red curve and the other two becomes significantly larger. Similarly, Figure 4c shows the development of number of clogged pores at ϕ=4.39%. The number of trapped particles decreases with bed depth. After 100 s, the particle number reaches a plateau in middle and lower regions, but still increases in top region. This is a clear sign of formation of cake filter. Similar shift of particle deposition distribution at different concentrations has also been noticed by *Wu and Huang* [2000].

Figure 4d shows one example of the correlation between flow rate and particle number at concentration ϕ=2.65%. In the experiment, the flow rate through the bypass hole is measured with a flowmeter and

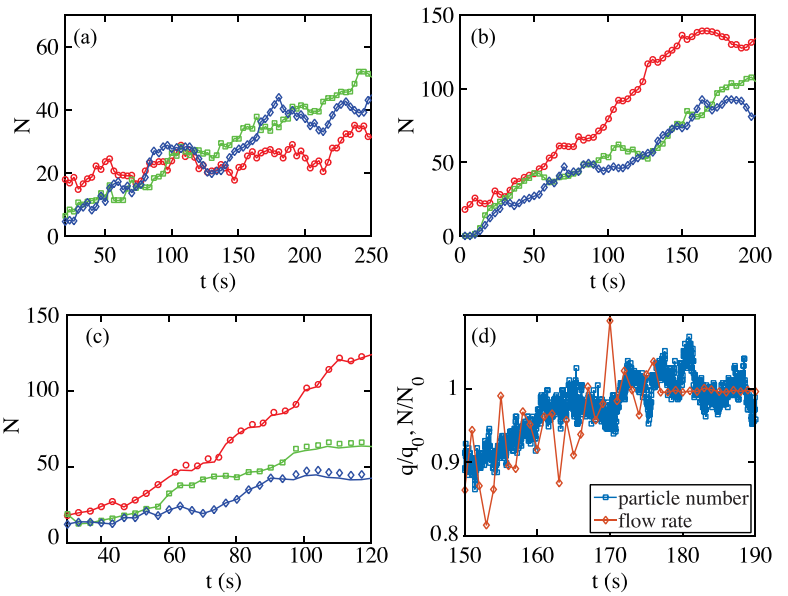

Figure 4. (a–c) The change of particle number N in each subvolume versus time at three different concentrations (a) ϕ=2.02%, (b) ϕ=2.65%, and (c) ϕ=4.39%. Three different colors of curves are corresponding to that of each boxes indicated in Figure 3. (d) The correlation between flow rate and particle number at concentration ϕ=2.65%.

shown in this figure, denoted as q. The total flow rate from the pump and particle tank is fixed at Q, so the flow rate through porous medium is $Q - q$. We choose to measure the flow through the bypass hole because it does not contain high concentration of particles as it is in the mainstream drained through the porous medium. If the particle number N increases with time, the permeability will decrease, which leads to a decrease of $Q - q$ and an increase of q. As the pressure head is kept the same, flow rate is directly linked to the hydraulic conductivity. To compare the trend of the number of clogged sites and the flow rate, N and q are normalized by their respective plateau values N_0 and q_0, which are obtained by averaging N and q from t = 185 to 190 s. The well-collapsed trend between two curves suggest that the particle number N has a strong correlation with the flow rate and thus the hydraulic conductivity. The flow rate curve shows some variations when $t < 180$ s. This does not necessarily represent the fluctuations of hydraulic conductivity, because the bypass hole is not completely immersed in water; some air is entrained into the tube, which might cause variations of flow rate.

Figure 5 shows the clogging patterns at the end of experiment after draining all water. These experiments were conducted at three different concentrations ϕ=2.02%, ϕ=2.65%, and ϕ=4.39%, which correspond

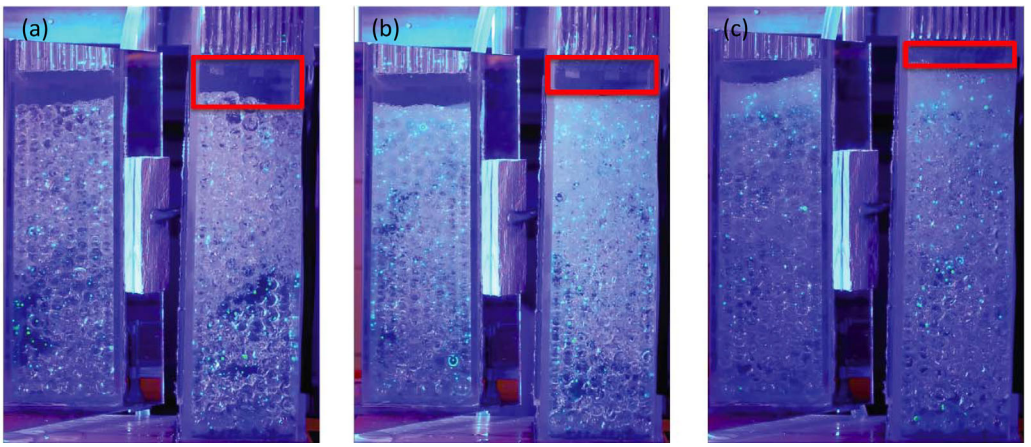

Figure 5. Clogging patterns at three different concentrations (a) ϕ=2.02%, (b) ϕ=2.65%, and (c) ϕ=4.39% after all water drained. The red boxes show the void space remaining and that indicates the cake filter thickness.

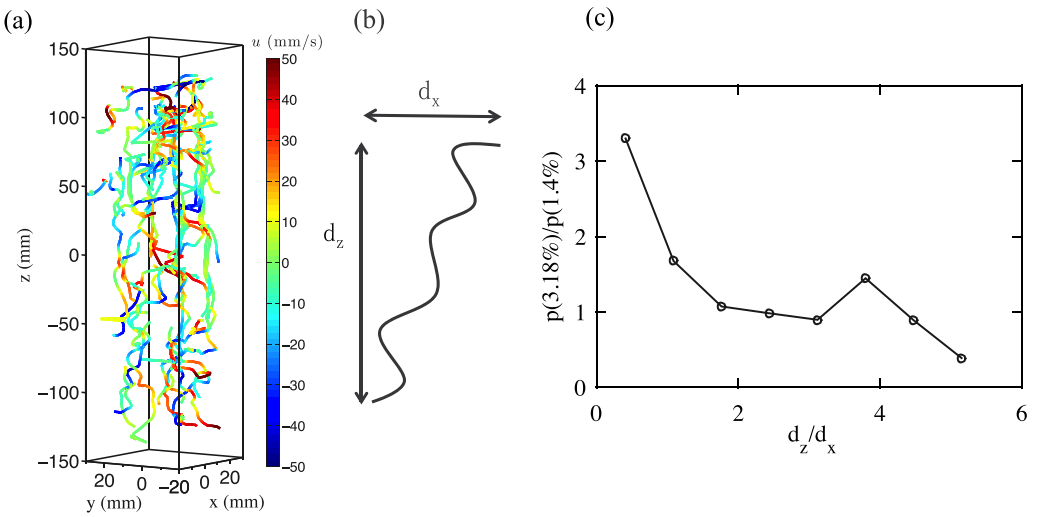

Figure 6. (a) The 3-D trajectories of dyed particles at ϕ=1.40% with color representing the transverse velocity along the x direction. (b) A cartoon of a particle trajectory with maximum displacement in transverse (d_x) and longitudinal direction (d_z) that are of interest. (c) The ratio of the two PDFs at ϕ=3.18% and ϕ=1.40%, p(3.18%)/p(1.40%).

to Figures 4a–4c. The red box in each panel shows the void space between the surface of porous bed and the upper bound of test section. Less void space indicates the presence of the filter cake above the packed beads. In Figure 5a, no filter cake is observed and the clogging is developed at the middle and lower region of the tank. It can also be noticed that the clogging sites formed at low concentration are not as dense as the ones at high concentrations. In Figures 5b and 5c, the clogging sites are so dense that the porous bed appears to be whiter compared with Figure 5a. At ϕ=2.65%, a thin layer of filter cake is formed on the top surface. The majority of particles are trapped within the upper half of the porous bed. At ϕ=4.39%, the filter cake is much thicker and most trapped particles are located close to the top of the porous medium. The observations in Figure 5 are consistent with the measurement in Figure 4 qualitatively. This suggests that the distribution of tracer particles is indeed representative of the clogging development in the porous medium.

In addition to positions of trapped particles, Figure 6a shows an example of many Lagrangian trajectories of moving particles at a concentration of ϕ=1.40%. Driven by the flow, fine particles typically preferentially move in the longitudinal direction when the concentration is so low that no pores are clogged. As soon as the clogging starts to develop, fine particles will be pushed to a different path to seek other open pores to pass, resulting in more transverse motions, which is illustrated in Figure 6b. To quantify this change, the ratio d_z/d_x between the maximum displacement in transverse x direction (d_x) and longitudinal z direction (d_z) of each trajectory is used. d_z/d_x can change from 0 to ∞. These two limits represent straight path along x and z directions, respectively. In our tracking experiments, this ratio is affected by the trajectory length. For example, if one long trajectory along the z direction is broken into three short segments. It will become three small values of d_z/d_x instead of one large value. Nevertheless, this bias will affect all concentrations, including ϕ=1.40% and ϕ=3.18%, consistently since their trajectory length distribution is the same. To remove this common trajectory length effects, Figure 6c shows the ratio of the two PDFs at ϕ=1.40% and ϕ=3.18%. Note that this ratio is extremely sensitive to any small variations of each PDF when they are close. We only show this PDF ratio for d_z/d_x below 6, above that it fluctuates around 1 suggesting that two PDFs are quite similar. This figure emphasizes the key differences between two concentrations: the large concentrations tend to have smaller d_z/d_x and therefore larger transverse migration. This means, statistically, there are more flow redirections due to clogging and that leads to more transverse motions of fine particles in search of open pores, which might be attributed to its faster clogging dynamics. In addition, this statistics is related to, but distinct from, the ratio (or the angle) between two velocity components w/u that has been used in many other studies [*Datta et al.*, 2013; *Kazemifar et al.*, 2015b]. Any statistics of Eulerian velocity are valuable to quantify the local flow information, but not necessarily help to determine the displacement that

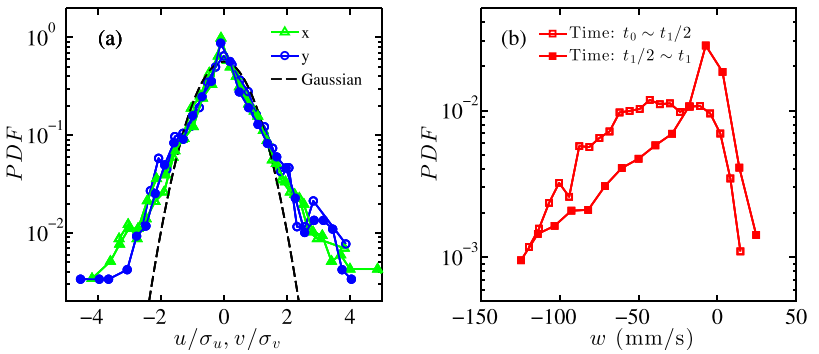

Figure 7. The PDFs of transverse and longitudinal velocities of tracked 1 mm particles at concentration ϕ=4.91% in the first half $t_0 \sim t_1/2$ (closed symbols) and the second half $t_1/2 \sim t_1$ (open symbols) of the entire clogging process. (a) The PDF of the transverse velocities normalized by their standard deviations compared with the Gaussian normal distribution indicated by the dashed line. (b) The PDF of the longitudinal velocity in the first half of the entire clogging process $t_0 \sim t_1/2$ and the second half $t_1/2 \sim t_1$.

takes place on a much larger timescale and length scale in the Lagrangian reference frame. This implies that this statistics of d_z/d_x is unique, and it can only be obtained using our particle tracking method.

Once the 3-D trajectories of particles are obtained, the velocity field is calculated utilizing a Gaussian velocity kernel with two functionalities: differentiation and smoothing [*Ni et al.*, 2012]. The normalized PDF of velocities in x and y direction are illustrated with different colors in Figure 7a at concentration ϕ=4.91%. The entire experiment is divided into two halves, the first half is for a porous medium with many open pores and the second one is for mostly clogged porous medium. The lines with open symbols show the velocity distribution in the first half.

In transverse direction, all four curves overlap very well and are symmetrical around $u = 0$ regardless of the system status. This proves that the porous medium used in this experiment is isotropic in transverse direction. Symmetric transverse velocity distributions have been studied in a clean porous medium before without clogging or high concentration of particles [*Moroni and Cushman*, 2001; *Huang et al.*, 2008; *Lachhab et al.*, 2008]. In these cases, it was found that the PDF follows a normal distribution. To compare, a Gaussian PDF curve is added to compare with the PDF of the transverse velocities in our study as indicated by the dashed line in Figure 7a. Although the distribution is quite close to Gaussian in the center, the tails are more intermittent. There are several explanations for this difference. First, the particle concentration is much higher in our experiments. The frequent particle-particle interactions will affect the velocity distributions significantly. Additionally, the particle sizes are different. In previous studies, tracers were small enough that they follows streamlines faithfully in the porous medium and their interactions with the pore and porous medium is negligible. In our study, however, the particle sizes are large enough to affect the surrounding flow and their interactions with the pore, such as temporary clogging and unclogging, will lead to more events of large transverse velocity.

Figure 7b shows the longitudinal velocities along the main flow z direction in the first half and second half of the clogging process as illustrated with different symbols. The velocity distributions are not only different from those in the transverse direction, but also very different with themselves during different stages in the clogging process. In the first half $t_0 \sim t_1/2$, the peak of PDF is around $u = -50$ mm/s, meaning the dominating flow direction is downward. In the second half $t_1/2 \sim t_1$, the peak shifts from -50 to 0, indicating more particles are trapped in clogged pores. However, the amount of particles with high speed ($>$120 mm/s) maintains the same and even increases a little bit. This is because some particles will flow at higher speeds due to local pressure buildup. In both stages, although dropping sharply, the PDF curves for $u > 0$ mm/s is not completely 0. Trapped particles may climb up and jump out of clogged pores via flow and pressure variations, which lead to positive longitudinal velocity.

4. Conclusion

In many environmental flow problems, including water resources management and subsurface oil and gas production, the flow through the porous medium is constantly contaminated by small particles, which lead

to complex filtration and clogging dynamics. In this paper, in order to visualize the entire clogging process, we developed a low-cost, 3-D-RIM-LPT system in a homogeneous porous medium. By tracking a small subset of fine particles we obtained 3-D particle trajectories and their statistics over the entire process at different particle concentrations. We observe that when the system gets clogged, the flow has to be redirected, and, as a result, the fine particles experience a more tortuous flow and travel in longer transverse paths until either they get trapped in one of the clogged pore or they find a path to get out of the porous medium. In addition, the pressure in the remaining open ones keeps increasing as more pores clogged. This is supported by the observation of a long tail at the high velocity in the vertical velocity PDF, suggesting large velocity of escaped particles from the open pores. It is also important to point out that the non-Darcy effect or the inertial effect in our system is larger than that in many applications, in which the permeability is significantly lower and size of both the grain and fine particles are much smaller. But at least for straining mechanism, we hypothesizes that the key parameter is the ratio between grain size and fine particle size rather than their physical sizes or the resulting Reynolds number. A detailed research is needed in future in order to test this hypothesis.

Acknowledgments
Financial support for this project was provided by Department of Mechanical and Nuclear Engineering, Pennsylvania State University. We would also like to thank Jhi Yong Loke, Ashik Ullah Mohammad Masuk, and Ashwanth Kumar Reddy Salibindla for their assistance in the experiment. Supporting data are included as one video in an SI file; any additional data may be obtained from R.N. (e-mail: rxn5006@engr.psu.edu).

References

Auset, M., and A. A. Keller (2006), Pore-scale visualization of colloid straining and filtration in saturated porous media using micromodels, *Water Resour. Res.*, *42*, W12S02, doi:10.1029/2005WR004639.

Berryman, J. G. (1983), Random close packing of hard spheres and disks, *Phys. Rev. A*, *27*(2), 1053.

Bradford, S. A., S. R. Yates, M. Bettahar, and J. Simunek (2002), Physical factors affecting the transport and fate of colloids in saturated porous media, *Water Resour. Res.*, *38*(12), 1327, doi:10.1029/2002WR001340.

Chen, C., A. I. Packman, D. Zhang, and J.-F. Gaillard (2010), A multi-scale investigation of interfacial transport, pore fluid flow, and fine particle deposition in a sediment bed, *Water Resour. Res.*, *46*, W11560, doi:10.1029/2009WR009018.

Chilton, T. H., and A. P. Colburn (1931), II—Pressure drop in packed tubes 1, *Ind. Eng. Chem.*, *23*(8), 913–919.

Corapcioglu, M. Y., and A. Haridas (1984), Transport and fate of microorganisms in porous media: A theoretical investigation, *J. Hydrol.*, *72*(1–2), 149–169.

Datta, S. S., H. Chiang, T. Ramakrishnan, and D. A. Weitz (2013), Spatial fluctuations of fluid velocities in flow through a three-dimensional porous medium, *Phys. Rev. Lett.*, *111*(6), 064501.

Dijksman, J. A., F. Rietz, K. A. Lőrincz, M. van Hecke, and W. Losert (2012), Invited article: Refractive index matched scanning of dense granular materials, *Rev. Sci. Instrum.*, *83*(1), 011301.

Drummond, J. D., R. J. Davies-Colley, R. Stott, J. P. Sukias, J. W. Nagels, A. Sharp, and A. I. Packman (2015), Microbial transport, retention, and inactivation in streams: A combined experimental and stochastic modeling approach, *Environ. Sci. Technol.*, *49*(13), 7825–7833.

Fukushima, E. (1999), Nuclear magnetic resonance as a tool to study flow, *Annu. Rev. Fluid Mech.*, *31*(1), 95–123.

Ginn, T. R., B. D. Wood, K. E. Nelson, T. D. Scheibe, E. M. Murphy, and T. P. Clement (2002), Processes in microbial transport in the natural subsurface, *Adv. Water Resour.*, *25*(8), 1017–1042.

Hajra, M., L. Reddi, L. Glasgow, M. Xiao, and I. M. Lee (2002), Effects of ionic strength on fine particle clogging of soil filters, *J. Geotech. Geoenviron. Eng.*, *128*(8), 631–639.

Huang, A. Y., M. Y. Huang, H. Capart, and R.-H. Chen (2008), Optical measurements of pore geometry and fluid velocity in a bed of irregularly packed spheres, *Exp. Fluids*, *45*(2), 309–321.

Hunt, J. R., B. C. Hwang, and L. M. McDowell-Boyer (1993), Solids accumulation during deep bed filtration, *Environ. Sci. Technol.*, *27*(6), 1099–1107.

Ives, K. (1970), Rapid filtration, *Water Res.*, *4*(3), 201–223.

Kau, S. M., and D. F. Lawler (1995), Dynamics of deep-bed filtration: Velocity, depth, and media, *J. Environ. Eng.*, *121*(12), 850–859.

Kazemifar, F., G. Blois, D. C. Kyritsis, and K. T. Christensen (2015a), A methodology for velocity field measurement in multiphase high-pressure flow of CO_2 and water in micromodels, *Water Resour. Res.*, *51*, 3017–3029, doi:10.1002/2014WR016787.

Kazemifar, F., G. Blois, D. C. Kyritsis, and K. T. Christensen (2015b), Quantifying the flow dynamics of supercritical CO_2–water displacement in a 2D porous micromodel using fluorescent microscopy and microscopic PIV, *Adv. Water Resour.*, *95*, 352–368.

Kutsovsky, Y., L. Scriven, H. Davis, and B. Hammer (1996), NMR imaging of velocity profiles and velocity distributions in bead packs, *Phys. Fluids*, *8*(4), 863–871.

Lachhab, A., Y.-K. Zhang, and M. V. Muste (2008), Particle tracking experiments in match-index-refraction porous media, *Ground Water*, *46*(6), 865–872.

Leis, A. P., S. Schlicher, H. Franke, and M. Strathmann (2005), Optically transparent porous medium for nondestructive studies of microbial biofilm architecture and transport dynamics, *Appl. Environ. Microbiol.*, *71*(8), 4801–4808.

Mackie, R., and R. Bai (1992), Suspended particle size distribution and the performance of deep bed filters, *Water Res.*, *26*(12), 1571–1575.

McDowell-Boyer, L. M., J. R. Hunt, and N. Sitar (1986), Particle transport through porous media, *Water Resour. Res.*, *22*(13), 1901–1921.

Molnar, I. L., W. P. Johnson, J. I. Gerhard, C. S. Willson, and D. M. O'Carroll (2015), Predicting colloid transport through saturated porous media: A critical review, *Water Resour. Res.*, *51*(9), 6804–6845.

Moroni, M., and J. H. Cushman (2001), Statistical mechanics with three-dimensional particle tracking velocimetry experiments in the study of anomalous dispersion. II. Experiments, *Phys. Fluids*, *13*(1), 81–91.

Ni, R., S.-D. Huang, and K.-Q. Xia (2012), Lagrangian acceleration measurements in convective thermal turbulence, *J. Fluid Mech.*, *692*, 395–419.

O'Melia, C. R., and W. Ali (1978), The role of retained particles in deep bed filtration, *Prog. Water Technol.*, *10*(3), 176–182.

Ouellette, N. T., H. Xu, and E. Bodenschatz (2006), A quantitative study of three-dimensional Lagrangian particle tracking algorithms, *Exp. Fluids*, *40*(2), 301–313.

Porter, K. E., et al. (1989), An overview of formation damage (includes associated paper 20014), *J. Pet. Technol.*, *41*(08), 780–786.

Putze, T. (2005), Geometric modelling and calibration of a virtual four-headed high speed camera-mirror system for 3-D motion analysis applications, in *7th Optical 3-D Measurement Techniques*, pp. 167–174, Vienna, Austria.

Rajagopalan, R., and C. Tien (1976), Trajectory analysis of deep-bed filtration with the sphere-in-cell porous media model, *AIChE J.*, *22*(3), 523–533.
Rodgers, M., J. Mulqueen, and M. G. Healy (2004), Surface clogging in an intermittent stratified sand filter, *Soil Sci. Soc. Am. J.*, *68*(6), 1827–1832.
Sakthivadivel, R., and H. A. Einstein (1970), Clogging of porous column of spheres by sediment, *J. Hydraul. Div.*, *96*(2), 461–472.
Seidler, G., G. Martinez, L. Seeley, K. Kim, E. Behne, S. Zaranek, B. Chapman, S. Heald, and D. Brewe (2000), Granule-by-granule reconstruction of a sandpile from x-ray microtomography data, *Phys. Rev. E*, *62*(6), 8175.
Song, C., H. Park, and K. Lee (2006), Experimental study of filter clogging with monodisperse PSL particles, *Powder Technol.*, *163*(3), 152–159.
Wiederseiner, S., N. Andreini, G. Epely-Chauvin, and C. Ancey (2011), Refractive-index and density matching in concentrated particle suspensions: A review, *Exp. Fluids*, *50*(5), 1183–1206.
Wildenschild, D., C. Vaz, M. Rivers, D. Rikard, and B. Christensen (2002), Using x-ray computed tomography in hydrology: Systems, resolutions, and limitations, *J. Hydrol.*, *267*(3), 285–297.
Willis, M. S., and I. Tosun (1980), A rigorous cake filtration theory, *Chem. Eng. Sci.*, *35*(12), 2427–2438.
Willneff, J., and H.-G. Maas (2000), *Design and Calibration of a Four-Headed Camera System for Use in Microgravity Research*, Vol. XXXIII, ETH Zurich, Inst. of Geod. and Photogramm, Amsterdam.
Wu, F.-C., and H.-T. Huang (2000), Hydraulic resistance induced by deposition of sediment in porous medium, *J. Hydraul. Eng.*, *126*(7), 547–551.
Yao, K.-M., M. T. Habibian, and C. R. O'Melia (1971), Water and waste water filtration. Concepts and applications, *Environ. Sci. Technol.*, *5*(11), 1105–1112.